J Electr Eng Technol.2017; 12(4): 1503-1510
http://doi.org/10.5370/JEET.2017.12.4.1503

ISSN(Print) 1975-0102
ISSN(Online) 2093-7423

Thermal Analysis of a High Speed Induction Motor Considering Harmonic Loss Distribution

Minh-Trung Duong*,, Yon-Do Chun*,**, Byoung-Gun Park*,**, Dong-Jun Kim*, Jae-Hak Choi* and Pil-Wan Han†**

Abstract – In this paper, a thermal analysis of a high speed induction motor with a PWM voltage source was performed by considering harmonic loss components. The electromagnetic analysis of the high speed induction motor was conducted using the time-varying finite element method, and its thermal characteristics were carried out using the lump-circuit method. Harmonic losses from tests in the high frequency region were divided into core loss and conductor loss components using various ratios, in order to determine the loss distributions for the thermal analysis. The results from both the calculations and experiment were validated using a high speed induction motor prototype operating at 20,000rpm.

Keywords: High speed, Induction motor, Thermal analysis, Lumped parameter, Harmonic loss

1. Introduction

In the field of electric machine design, thermal analysis is usually neglected, or is considered in the context of current density. That approach is acceptable for small and medium sized or low speed machines, but it will not provide an exact temperature. In a high speed machine, high rotor speeds or high electrical frequencies will lead to higher losses in iron and copper, and cause an increase in temperature [1]. And with the increasing demand for miniaturization, energy efficiency, and cost reduction as well as the drive to fully exploit new technologies and materials, it has now become necessary to analyze the thermal design of a circuit to the same extent as the electro-magnetic design [2].

There are several well-known approaches for such thermal analysis, including the finite element method (FEM), computational fluid dynamics (CFD) and lumped parameter thermal-network (LPTN). The biggest advantage of the thermal finite element model is it provides an accurate calculation of conducted heat in complex geometric shapes. Specifically, FEM can provide a fairly accurate picture of temperature distribution in the complex solid parts of a machine [3-5]. However, the main shortcoming of this approach is the need to make certain assumptions about the placements of conductors, and the given temperature for any open boundaries [6]. In addition, FEM calculations are time-consuming, even when a parametric approach is used to define the geometry.

† Corresponding Author: Electric Motor Research Center, Korea Electrotechnology Research Institute. (pwhan@keri.re.kr)
* Electric Motor Research Center, Korea Electrotechnology Research Institute.
** Dept. of Energy and Power Conversion Engineering, Korea University of Science & Technology, Changwon, Korea
Received: March 10, 2017; Accepted: March 27, 2017

The CFD approach has been used in a wide range of heat exchange analyses, from photovoltaic thermal system to concentric-tube heat exchangers, and also high speed machine design [7-9]. The main strength of the CFD approach is that any new thermal can be analyzed [9] to determine coolant flow rate, velocity, and pressure distribution in the cooling passages, or around the machine, as well as the levels of heat transfer, which can be used in a subsequent analysis of temperature in the active material and remaining solid structures [2].

There are a large number of published studies about the LPTN approach, which consider the selection of suitable parameters [10-13]. As is well known, it is possible to lump together components that have similar temperatures and to represent each as a single node in the network. Nodes are separated by thermal resistances which represent the main heat-transfer paths, such as from the winding copper to the stator tooth, from the tooth and stator back iron nodes to stator bore and housing interface, etc. [2].

The critical problem in the thermal analysis of high speed machines is separating the harmonic loss components, which are difficult to determine because of their dependence on frequency and flux density. The required ranges of frequency and the flux density needed to calculate core losses in rotating machines are very wide [14]. J. V. Gragger *et al.* [15] summarized that under low switching frequencies, the biggest parts of the PWM harmonics losses are the harmonic rotor copper losses. K. Bradley *et al.* [16] provided a typical experimental separation of a harmonic loss curve under a full load, which showed that in the high switching frequency region, the percentage of core losses over total harmonic losses are increased significantly, while conductor losses plummet.

This paper focuses on the thermal analysis of a high speed 20,000rpm, 37kW induction motor under a PWM

voltage source using the LPTN approach. The basic loss components of a sinusoidal voltage supply were tested following the loss segregation method in IEC 60034-2-1, and harmonic loss was determined by calculating the difference in total loss between a sinusoidal and PWM supply, which were separated into components for the thermal analysis. Finally, these harmonic loss values were applied to the LPTN network to analyze motor temperature.

In order to validate the analysis results and calculated data, temperature measurements of the induction motor prototype were performed.

2. Loss Analysis and Test of High Speed Motor

2.1 Specification of the motor

The specifications of the studied motor are listed in Table 1, and the basic design of the induction motor is described in Fig. 1. The motor is composed of a centrifugal casting copper rotor, a core made of electric steel and a water jacket for the cooling system, which should be considered as an important factor. Fig. 2 presents the relationship between the output power and torque versus rotating speed. It can be clearly seen that at a given torque value, the output power linearly increases with the rated speed and reaches the rated power of 37kW at 20,000 rpm.

Table 1. Specification of the high speed motor

Items	Unit	Rated	Maximum
Power	kW	37	
Rated line voltage	V	380	
Rated frequency	Hz	334	
Rated speed	RPM	20,000	
Cooling condition	Water cooling		

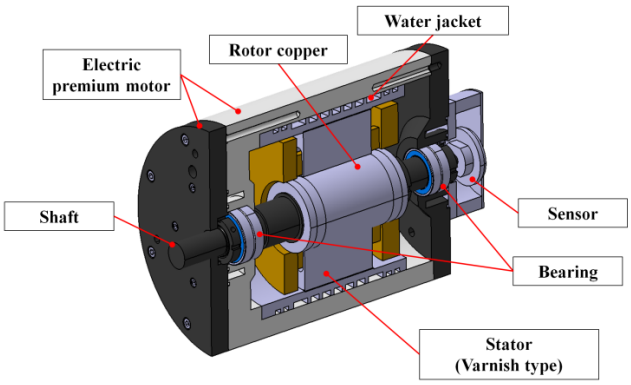

Fig. 1. Basic design of the 37kW high speed induction motor

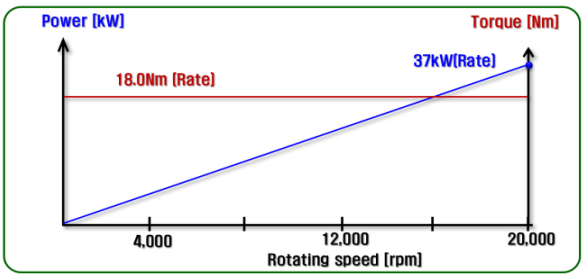

Fig. 2. Rated performance vs speed

2.2 Design of the motor

An overview of the high speed induction motor is provided in Fig. 3. The designed motor is composed of a rotor with 28 copper bars and stator with 24 slots. Both the stator and rotor core are made of electric steel 35PN250 from POSCO company [17]. The winding is designed with a 3 phase delta connection and 2 parallel conductors per slot. Also, water was selected for the cooling system. For the analysis, under operating conditions, the rated speed was controlled at 20,000rpm, and line-line input voltage was 380V.

The details of the geometry are presented in Table 2.

2.3 PWM voltage supply

The PWM waveform depends on the control unit and the

Table 2. Design of the high speed motor

Items	Unit	Value
Outer diameter of stator	mm	191
Inner diameter of stator	mm	83
Airgap	mm	1
Stacking length	mm	100
Number of phase	3	
Number of pole	2	
Number of stator/rotor slot	24/28	
Winding connection	Delta	
Core material	35PN250	
Rotor conductor material	Copper	

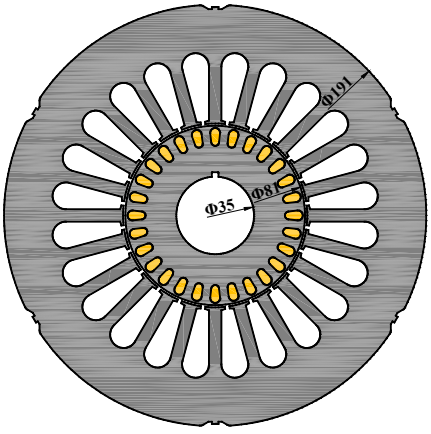

Fig. 3. Overview of high the speed induction motor

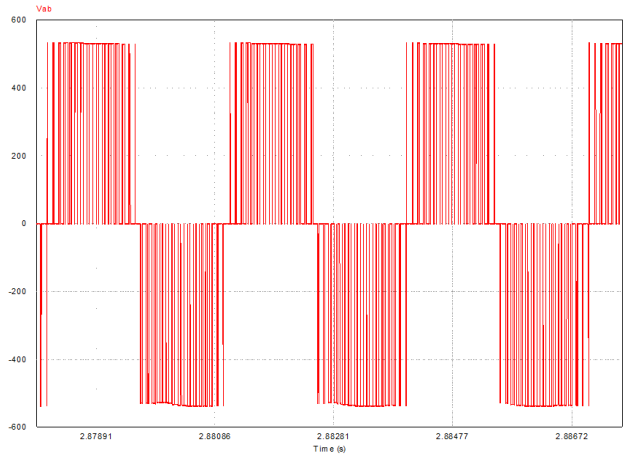

Fig. 4. Terminal voltage waveform (PWM)

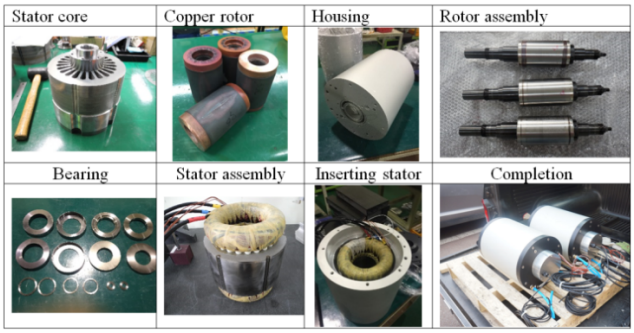

Fig. 5. Assembling prototype

converter topology. In this study, the space vector PWM was applied, which is the most commonly used PWM method.

2.4 Prototype assembling process

Fig. 5 shows the process assembling prototype. The rotor bars were made by centrifugal copper casting.

2.5 Loss analysis and test results

The basic losses, such as copper loss and iron loss, were calculated using a 2D electro-magnetic FEM with sinusoidal voltage.

Fig. 6 shows the flux density distribution of the designed models when excited by a sinusoidal waveform. The maximum values of the stator yoke and teeth flux density were 1.4[T] and 1.8[T], respectively.

The stator winding and rotor bar temperature were set on 90°C and 150°C. The stray loss was calculated to be about 1.0% of the output power, and the mechanical loss was calculated by using Takeuchi's formula [29].

Tests of the prototype using a sinusoidal supply were conducted by following IEC 60034-2-1, the loss segregation

Table 3. Test and FEM results

Supply	Copper loss (W)		Core loss (W)	Stray loss (W)	Mechanical loss (W)	Total loss (W)
	Stator	Rotor				
FEM (Sin.)	462	318	395	370	351	1896
TEST (Sin.)	390	460	452	300	140	1742
TEST (PWM)	3092 (Total Loss)					

Table 4. Harmonic loss separation cases taken from experimental data for the thermal analysis

Supply		Core loss (W)		Copper loss (W)	
		Stator	Rotor	Stator	Rotor
PWM	Case 1	538	137	325	350
	Case 2	750	190	195	215
	Case 3	915	230	98	107
	Case 4	970	245	65	70

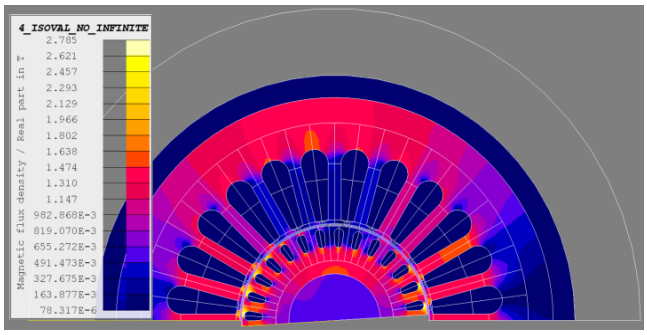

Fig. 6. Flux density distribution

method by means of output power. The PWM supply test was performed with an input-output method, and only total losses, including harmonic loss, were evaluated, as shown in Table 3. It can be calculated by using the difference (1350W) between the total losses for the sinusoidal and PWM voltage supply.

Investigations of harmonic loss components have been carried out in several studied cases. Two of the harmonic loss components, representing low-frequency and high frequency components, are primarily associated with conductor and core losses, respectively [13-16].

In the Table 4, harmonic losses are separated into copper loss and core loss using assumed ratios (harmonic copper loss/total harmonic loss) of 50%, 30%, 15% and 10%. The distribution of harmonic rotor copper loss over total harmonic copper loss, and harmonic rotor iron loss over total harmonic iron loss, were assumed of 20% and 52%. Each of the harmonic loss components in Table 4 were applied to the LPTN in the thermal analysis with sinusoidal losses, as shown in Table 3 in Chapter 3.

3. Parameter Calculations

3.1 Lumped parameter thermal network (LPTN) method

The LPTN method has been successfully used for thermal analysis of electric motors using commercial software as shown in [18]. All of the thermal parameters, such as conduction (R_c), radiation (R_r), convection thermal resistances (R_{cv}) and flow resistance (R_f) in the case of forced convection heat transfer are calculated by the program, while considering the cooling system as shown in Eqs. (3)~(6) [2].

$$R_c = \frac{L}{kA} \tag{3}$$

$$R_r = \frac{1}{h_R A} \tag{4}$$

$$R_{cv} = \frac{1}{h_C A} \tag{5}$$

$$R_f = \frac{k\rho}{2A^2} \tag{6}$$

where L is the path length, A is the path or surface area, k is the thermal conductivity, h_R is the heat-transfer coefficient, h_C is the convection-heat-transfer coefficient and ρ is the air or fluid density depending on the temperature.

3.2 Analysis of forced convection (water jacket)

In this study, a water jacket liquid cooling method was used, as shown in Fig. 6. In a forced convection system, if the fluid velocity is large, the turbulence is induced. The magnitude of Re (Reynolds number) in Eq. (7) is used when there is laminar or turbulent flow in a forced convection system [19~23]. Re was calculated to be 13,140 in this model. For a fully developed turbulent flow ($3{,}000 < Re < 10^6$), the Nu (Nusselt number) and heat transfer coefficient are calculated by Eqs. (9) and (10) [24].

$$Re = \rho \cdot v \cdot L / \mu \tag{7}$$

$$Pr = c_p \cdot \mu / k \tag{8}$$

$$Nu = \frac{f}{8} \cdot \frac{(Re - 1000) \cdot Pr}{1 + 12.7 \cdot (f/8)^{0.5} \cdot (Pr^{2/3} - 1)} \tag{9}$$

$$Nu = h \cdot L / k \tag{10}$$

where Pr is the Prandtl number, v is the fluid velocity [m/s], c_p is the fluid specific heat capacity [kJ/(kg· ℃)], μ is the fluid dynamic viscosity [kg/m/s], and f is the friction factor [19].

3.3 Analysis of forced convection (Air Gap)

The traditional method of accounting for heat transfer across an air gap is to use the dimensionless convection correlations developed by Tayler by testing on smooth concentric rotating cylinders [19, 25]. In order to determine whether the flow in the air gap is laminar, vortex or turbulent, the Taylor number (Ta) has to be calculated using Eq. (11). The flow is laminar if $Ta < 41$. If $41 < Ta < 100$ (our model: 79.5), the flow takes on a vertex form and Eq. (12) has to be used to calculate Nu [19].

$$Ta = Re \cdot (l_g / R_r)^{0.5} \tag{11}$$

where l_g is the air gap radial thickness, R_r is the rotor outer radius, and $Re = l_g \cdot v/\mu$

$$Nu = 0.202 \cdot (Ta)^{0.63} \cdot (Pr)^{0.27} \tag{12}$$

3.4 Critical parameters

The accuracy of the thermal networks is dependent on several parameters for which reliable data may be difficult to find. These include, for example, the interface gap between components and the thermal conductivity of the important materials used in the electrical motors [26]. It is difficult to find appropriate thermal data for electrical steel, insulation and impregnation materials. Table 5 shows the thermal conductivity values of these materials used in this thermal analysis. It was assumed that electrical steel contains 1.5% silicon because that value is not released by manufacturer.

The accuracy of a prediction of a motor's thermal performance is also dependent on the estimates of the many thermal contact resistances within the machine (stator lamination to housing, slot-liner to lamination, etc) [27].

The data given by Mills [28] can be converted to equivalent air gaps by using a thermal conductivity value for air of 0.026 W/m/C. For the typical material interfaces found in electrical machines, the values of an interface gap for aluminum-aluminum are in the range

Table 5. Thermal conductivity of important materials

Material	Thermal Conductivity [W/m/℃]	Remarks
Electrical steel	33	Silicon 1.5 %
Epoxy	1.02	Molding of windings
Nomex 410	0.14	Slot liner
Aluminum	168	Housing

0.0005 to 0.0025 mm and for aluminum-iron of 0.0006 to 0.006 mm [28]. The gap between the lamination and housing is a function of how well the rough laminated outer surface of the stator has been prepared before the housing is fitted. This study used 0.01mm as the gap between the lamination and aluminum housing considering the roughness of the lamination.

4. Thermal Analysis and Test Results

4.1 Parameters for the thermal analysis

Table 6 shows the heat transfer coefficients of the important parts, and the thermal resistances determined by commercial software using the theory presented in Chapter 3.

In this study, because the high speed motor is a water cooling type, the heat transfer coefficients of the water jacket channel and the interface between the stator core and frame are dominant.

Table 6. Heat transfer coefficient of important parts

Components	Heat tran. coef. [W/m²/℃]	Remarks
Air gap	128.1	Convection
Water jacket channel	6,997	Convection
From end coil to inner air	133	Convection
From end ring to inner air	210	Convection
From housing to outer air	8.3	Conv.+Rad.
Between stator core and frame	2,600	Interface gap

Table 7. Comparison between simulation and experiment

	End winding temperature (℃)		
Voltage supply	Experiment	Simulation	Accuracy (%)
Sinusoidal	74.20	73.50	99.06
PWM Case 1	101.5	116.4	85.32
PWM Case 2	101.5	112.5	89.16
PWM Case 3	101.5	109.6	92.02
PWM Case 4	101.5	102.7	98.82

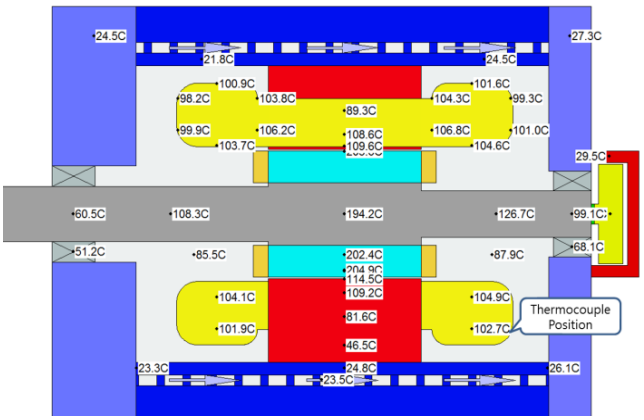

Fig. 7. Temperature distribution (Test losses)

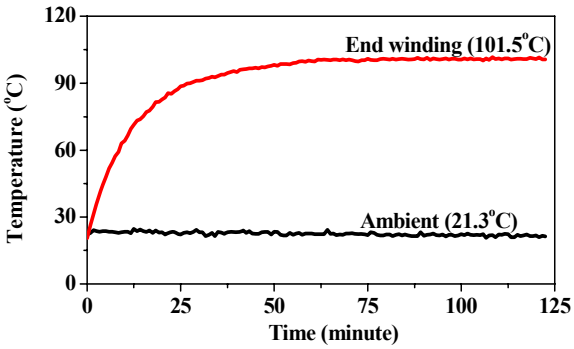

Fig. 8. Temperature saturation test

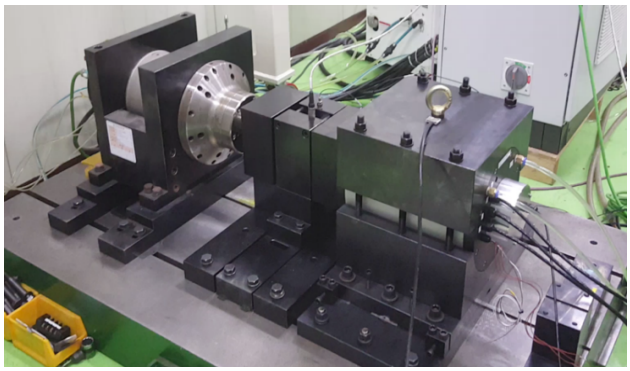

Fig. 9. Dynamo system used for testing

4.2 Analysis results and comparison with test results

The calculated temperature of the end winding was determined by applying loss data from the four different cases in Chapter 2.5 and the thermal parameters from Chapter 3 into Motor CAD, a commercial software for the LPTN method. In Table 7, the comparison between the simulated and experimental data verifies the proposed assumption that under high frequency operation, the majority loss component is iron loss, while copper loss just account for a relatively small percentage. If the harmonic copper loss is assumed to be 50%, the accuracy is around 85.3%. The accuracy of the temperature analysis increases significantly to over 98% when harmonic copper losses ratio is assumed to be 10%.

Fig. 7 shows the temperature distribution as determined by the thermal analysis results for case 4 using the LPTN method. The test results for the motor temperature are from the temperature saturation test of Fig. 8, using the 60kW Dynamo system shown in Fig. 9.

The difference between stator and rotor temperature is high, over 100°C, which is why this model is a housing water cooling type (as per the cooling water condition in Table 1).

If harmonic losses are separated accurately by loss segregation test and the interface gap between the housing and lamination or the equivalent thermal conductivity between the winding and lamination is adjusted, the winding temperature in the slot can be calculated accurately.

5. Conclusion

This paper studied the use of estimated loss components, obtained from simulations and experimental data and several assumptions, for the thermal analysis of an electric machine. The thermal analysis of a water cooling type, high speed induction motor under a PWM voltage supply, using the analytical lumped-circuit method, is shown in [18]. In addition to critical parameters such as the interface gap between the materials and the thermal conductivity of important materials, loss components were important factors for accurately calculating the temperature distribution of a high speed induction motor using a PWM supply and the LPTN method. The validation of the thermal analysis confirmed its excellent accuracy, as the copper loss component of the harmonic losses was found to be relatively small. In next step, harmonic loss distributions will be defined accurately by loss segregation test following IEC-60034-2-3, the results can be applied to thermal analysis.

Acknowledgment

This work was supported by the Korea Institute of Energy Technology Evaluation and Planning (KETEP) and the Ministry of Trade, Industry & Energy (MOTIE) of the Republic of Korea (No. 20152010103410).

References

[1] S. Nategh, "Thermal Analysis and Management of High-Performance Electrical Machines," Doctoral Thesis, Stockholm, Sweden, 2013.

[2] A. Boglietti, A. Cavagnino and D. Staton, "Evolution and Modern Approaches for Thermal Methods Analysis of Electrical Machines," *IEEE Trans. on Industrial Elec*., vol. 56, no. 3, pp. 249-255, Jan./Feb., 2010.

[3] S. Nategh, O. Wallmark, M. Leksell and S. Zhao, "Thermal Analysis of a PMaSRM Using Partial FEA and Pumped Parameter Modeling," *IEEE Trans. on Energy Conv*., vol. 27, no. 2, Jun., 2012.

[4] M. Popescu, D. G. Dorrell, L. Alberti, N. Bianchi, D. A. Staton, and D. Hawkins, "Thermal Analysis of Duplex Three-Phase Induction Motor Under Fault Operating Conditions," *IEEE Trans. on Industrial Appl*., vol. 49, no. 4, Jul/ Aug., 2013.

[5] W. Le, J. Cao and X. Zhang, "Electromechanical Analysis of Induction Motor with Compound Cage Rotor Used for PHEV," *IEEE Trans. on Industrial Elec*., vol. 57, no. 2, Feb., 2010.

[5] Motor-CAD. [Online]. Available: www.motor-design.com

[6] Flux-2D tutorial technical, "Electromagnetic and Thermal Analysis of a Brushless IPM motor by multi-physics coupling".

[7] A. A. B. Baloch, H. M. S. Bahaidarah and P. Gandhidasan, "Computational Fluid Dynamics Study for the Optimization of Surface Temperature Profile of Photovoltaic / Thermal System," Photovoltaic Specialists Conference (PVSC), 2016 IEEE 43rd.

[8] A. Boglietti, A. Cavagnino, and D. Staton, "TEFC induction thermal models: A parameters sensitivity analysis," *IEEE Trans. Ind. Appl*., vol. 41, no. 3, pp. 756-763, May/Jun., 2005.

[8] T. W. Choon, M. S. Shariff and M. Law, "Computational Fluid Dynamics Analysis of Shell-and-double Concentric-tube Heat Exchanger," *IEEE Symposium on Industrial Electronics and Applications (ISIEA2011)*, Sept. 25-28, 2011.

[9] R. Vlach and R. Huzlik, "Thermal Model of High Speed Asynchronous Machine," 17th International Conference on Mechatronics – Mechatronika (ME), 2017.

[10] G. G. Gueno, P. Chantrenne and J. Jac, "Parameter Identification of a Lumped Parameter Thermal Model for a Permanent Magnet Synchronous Machine," Electric Machines & Drives Conference (IEMDC), 2013 IEEE International.

[11] F. Qi, M. Schenk and R. W. De Doncker, "Discussing Details of Lumped Parameter Thermal Modeling in Electrical Machines," 7th IET International Conference on Power Electronics, Machines and Drives (PEMD 2014).

[12] O. Wallscheid and J. Bockner, "Design and Empirical Identification of a Lumped Parameter Thermal Network for Permanent Magnet Synchronous Motors with Physically Motivated Constrains," Electric Machines & Drives Conference (IEMDC), 2015 IEEE International.

[13] P. W. Han, J. H. Choi, D. J. Kim, Y. D. Chun and D. J. Bang, "Thermal Analysis of High Speed Induction Motor by Using Lumped-Circuit Parameter," *J Electr. Eng. Techol.2015*., vol. 10, no. 5, pp. 709-718, 2015.

[14] K. Yamazaki, A. Suzuki, M. Ohto and T. Takakura, "Harmonic Loss and Torque Analysis of High-Speed Induction Motors," *IEEE Trans. Ind. Applicat*., vol. 48, no. 3, May/Jun. 2012.

[15] J. V. Gragger, A. Haumer, C. Kral and F. Pirker, "Efficient Analysis of Harmonic Losses in PWM Voltage Source Induction Machine Drives with

Modelica," Modelica 2008, Mar. 3rd – 4th, 2008.
[16] K. Bradley, W. Cao, J. Clare and P. Wheeler, "Predicting Inverter-Induced Harmonic Loss by Improved Harmonic Injection," *IEEE Trans. Power Electron*., vol. 23, no. 5, Sep. 2008.
[17] www.posco.co.kr/homepage/docs/eng3/html/company/product/s91e7010010c.jsp
[18] Motor-CAD. [Online]. Available: www.motor-design.com
[19] D. A. Staton and A. Cavagnino, "Convection heat transfer and flow calculations suitable for electric machines thermal models," *IEEE Trans. on Industrial Elec*., vol. 55, no. 10, pp. 3509-3516, Oct., 2008.
[20] D. W. Van De Pol and J. K. Tierney, "Free convection Nusselt number for vertical U-shaped channels," *Trans. ASME*, vol. 95, pp. 542-543, Nov. 1973.
[21] A. F. Mills, Heat Transfer. Englewood Cliffs, NJ: Prentice-Hall, 1999.
[22] C. D. Jones and L. F. Smith, "Optimum arrangement of rectangular fins on horizontal surfaces for free-convection heat transfer," *Trans. ASME*, vol. 92, pp. 6-10, Feb. 1970.
[23] F. Heiles, "Design and arrangement of cooling fins," *Elecktrotecknik und Maschinenbay*, vol. 69, no. 14, pp. 42-48, Jul. 1952.
[24] V. Gnielinski, "New equations for heat and mass transfer in turbulent pipe and channel flow," *Int. Chem. Eng*., vol. 16, pp. 359-368, 1976.
[25] G. I. Taylor, "Distribution of velocity and temperature between concentric cylinders," *Proc. Roy Soc*., vol. 159, pp. 546-578, 1935.
[26] A. Boglietti, A. Cavagnino and D. Staton, "Determination of Critical Parameters in Electrical Machine Thermal Models," *IEEE Trans. on Industry App*., vol. 44, no. 4, pp. 1150-1159, Jul./Aug., 2008.
[27] D. Staton, A. Boglietti and A. Cavagnino, "Solving the More Difficult Aspects of Electric Motor Thermal Analysis in Small and Medium Size Industrial Induction Motors," *IEEE Trans. on Energy Con*., vol. 20, no. 3, pp. 620-628, Sept., 2005.
[28] A. F. Mills, Heat Transfer. Englewood Cliffs, NJ: Prentice Hall, 1999.

Minh-Trung Duong He received the B.S. degrees in Electrical Engineering Department from Hanoi University of Science and Technology in 2014. Currently he is studying as a Ph.D. student in integrative program in Korea Electrotechnology Research Institute Campus, which belongs to Power and Energy Conversion Engineering Department, University of Science and Technology. His research interests include design and analysis of rotating machine and tubular generator, energy harvesting in applications to vehicle suspension systems.

Yon-Do Chun He received the B.S., M.S. and Ph.D. degrees in Electrical Engineering from Hanyang University in 1996, 1998 and 2001, respectively. From 2001 to 2003, he received a fellowship from the Japan Society for the Promotion of Science (JSPS), and he was with the Department of Electrical Engineering at Waseda University as a visiting scholar. From 2004 to 2012, he worked at the Korea Electrotechnology Research Institute (KERI). He is currently a chief researcher, Principal Researcher and technical leader of the Electric Motor Research Center, KERI.

Byoung-Gun Park He received his B.S. in Electrical Engineering from Myongji University, Yongin, Korea, in 2005, and his M.S. and Ph.D. in Electrical Engineering from Hanyang University, Seoul, Korea, in 2007 and 2011, respectively. Since 2011, he has been with the Korea Electrotechnology Research Institute (KERI), Changwon, Korea, where he is currently a Senior Researcher in the Electric Motor Research Center.

Dong-Jun Kim He received the B.S degree in Electrical Engineering in 2004 from Kyungnam University. He received the M.S degree in Electrical Engineering in 2013 from Changwon National University. He has worked at the Korea Electrotechnology Research Institute (KERI). He is currently a senior Engineer of the Electric Motor Research Center, KERI.

Jae-Hak Choi He received the B.S., M.S., and Ph.D. degrees in Electrical Engineering from Hanyang University in 1999, 2001 and 2005, respectively. From 2005 to 2007, he worked at LG electronics. Since 2008, he has worked at the Korea Electrotechnology Research Institute (KERI). He is currently a senior researcher of the Electric Motor Research Center, KERI.

Pil-Wan Han He received the B.S., M.S. and Ph.D. degrees in Electrical Engineering from Hanyang University in 1998, 2000 and 2013, respectively. From 2000 to 2005, he worked at LG electronics. Since 2005, he has worked at the Korea Electrotechnology Research Institute (KERI). He is currently a senior researcher of the Electric Motor Research Center, KERI.